Chemical Physics Letters 549 (2012) 67–71

Contents lists available at SciVerse ScienceDirect

Chemical Physics Letters

journal homepage: www.elsevier.com/locate/cplett

Effect of particle size on the magnetic properties of $Ni_xCo_{1-x}Fe_2O_4$ ($x \approx 0.3$) nanoparticles

K. Maaz [a,b], S. Karim [b], Gil-Ho Kim [a,*]

[a] School of Electronic and Electrical Engineering and Sungkyunkwan Advanced Institute of Nanotechnology (SAINT), Sungkyunkwan University, Suwon 440-746, Republic of Korea
[b] Nanomaterials Research Group, Physics Division, PINSTECH, Nilore, Islamabad, Pakistan

ARTICLE INFO

Article history:
Received 22 June 2012
In final form 21 August 2012
Available online 31 August 2012

ABSTRACT

$Ni_xCo_{1-x}Fe_2O_4$ ($x \approx 0.3$) nanoparticles were synthesized via chemical co-precipitation method. The particle size (d) was found to increase linearly with increasing annealing temperature. Magnetic studies revealed that the coercivity (H_C) attains a value of 965 Oe at ~18 nm and then decreases for larger particles. The behavior of H_C with d was attributed to the superparamagnetic nature of smaller nanoparticles, whereas for larger particles it was attributed to domain transformation mechanism. Both saturation magnetization (M_S) and superparamagnetic blocking temperature (T_b) were found to increase linearly with increasing size of the nanoparticles.

1. Introduction

Nanoparticles have attracted considerable attention owing to their interesting optical, electrical, chemical, and magnetic properties when compared with those of their bulk components [1–3]. These properties make them the focus of great scientific and technological interest, particularly in the biomedical, optical, and electronic fields [4–7]. The magnetic behavior of nanoparticles used in technological applications depends crucially on the size, shape, and purity of the materials. These particles should be in single-domain state, of pure phase, and must have optimized coercivity and saturation magnetization. Ferrite nanoparticles are the most suitable candidates for a variety of applications. The most significant properties of ferrite nanoparticles, namely, magnetic saturation, coercivity, and magnetization loss, change drastically as compared to their bulk counterparts [8,9]. Among the various ferrites that form a major constituent of magnetic ceramic materials, nanosize Ni- and Co-ferrite possess attractive properties as the soft and hard magnets and the low-loss magnetic materials at high frequencies [10]. In data storage and recording applications, magnetic nanoparticles with relatively high superparamagnetic blocking temperature are required, whereas in biomedical applications, nanoparticles with relatively low blocking temperature and moderate coercivity are required. Therefore, it is very important to tailor various magnetic properties in these materials according to their specific applications. This can be done either by varying the sizes of the nanoparticles or by adjusting the relative concentrations of the soft (e.g., Ni-ferrite) and hard (e.g., Co-ferrite) phases. Magnetism and its related phenomena in ferrite nanoparticles include surface and finite size effects, and interparticle interactions. In small-sized particles, the surface spins play a dominant role that causes, for example, reduction in saturation magnetization, enhancement in coercivity, and magnetic relaxation effects as the size of the particles decreases. In ferrite nanoparticles, due to the broken symmetries and exchange bonds at the surfaces, the surface spins do not follow the core anisotropy direction and become disordered or canted, thereby leading to an even high anisotropy as compared to the core anisotropy. Such nanoparticles are generally termed as the core–shell nanoparticles; here, the core-spins behave like ferro- or ferri-magnetic materials, whereas the shell is composed of disordered or canted spins.

In conventional nanoparticles preparation techniques, the control of size and size distribution of the particles is difficult [11]. This difficulty has been overcome by using the co-precipitation technique for synthesizing $Ni_{0.3}Co_{0.7}Fe_2O_4$ nanoparticles. In order to prevent the oxidation of the nanoparticles in atmospheric oxygen and to stop their agglomeration, the particles are coated with oleic acid that is used as the surfactant during the reaction [12]. The required size and size distribution is achieved by controlling the relative rate of nucleation and growth during the reaction process. Smaller and uniformly distributed particles are obtained if the nucleation rate is higher than the growth rate and vice versa. The advantage of this method over other methods is that it is relatively simpler, cost effective, and affords high yields with controlled crystallinity.

In this Letter, we report the effects of particle size on the magnetic properties of $Ni_{0.3}Co_{0.7}Fe_2O_4$ nanoparticles with sizes in the range 12–35 ± 3 nm. This is a detailed study of this kind for this particular concentration of Ni-doped cobalt ferrite

* Corresponding author.
E-mail address: ghkim@skku.edu (G.-H. Kim).

0009-2614/$ - see front matter © 2012 Elsevier B.V. All rights reserved.
http://dx.doi.org/10.1016/j.cplett.2012.08.041

(i.e. $Ni_{0.3}Co_{0.7}Fe_2O_4$). The results are explained with reference to the disordered surface spins, finite size effects, thermal activation model, and interparticle dipole–dipole interactions in magnetic nanoparticles.

2. Synthesis procedure

For the synthesis of $Ni_{0.3}Co_{0.7}Fe_2O_4$ nanoparticles, the chemical reagents used were nickel chloride, cobalt chloride, ferric chloride, sodium hydroxide, and oleic acid. All the chemicals were analytical grade and were used without further purification. Double distilled de-ionized water was used as the solvent. First, 0.4 molar (M) solution of iron chloride and 0.2 M of cobalt and nickel chloride were mixed together. 3 M solution of sodium hydroxide was added drop-wise to the mixture solution. The pH of the reaction was monitored constantly. The reactants were vigorously mixed until a pH level of ~12 was achieved. A specific amount of oleic acid (2–3 drops for 75 ml solution) was added as the surfactant. The reaction was carried out at ~80 °C under vigorous stirring for 1 h. The product was cooled to room temperature and washed twice with distilled water and subsequently with ethanol to remove the excess surfactant in the prepared nanoparticles. The sample was centrifuged for 15 min and dried overnight at above 80 °C. The acquired substance was subsequently ground into the fine powder and annealed for 6 h at various temperatures to obtain the required nanoparticles. The structure of the final product was investigated using X-ray diffraction (XRD) and transmission electron microscopy (TEM) analyses while magnetic characterization was performed by using the physical property measurement system (PPMS).

3. Results and discussion

Figure 1 shows the XRD pattern of the cubic $Ni_{0.3}Co_{0.7}Fe_2O_4$ nanoparticles according to JCPDF cards #742081 and 791744 shown for reference purposes. The XRD pattern confirms the presence of polycrystalline inverse spinel Ni–Co ferrite nanoparticles. From the XRD line broadening of the strongest (3 1 1) peak, the crystallite sizes were calculated using the Debye–Scherrer equation. Figure 2 shows the high-resolution TEM image of one sample annealed at 600 °C for 6 h. The TEM image shows that the particles are of spherical shape with an average size of 12 ± 3 nm. It was found that the crystallite size obtained from XRD analysis was

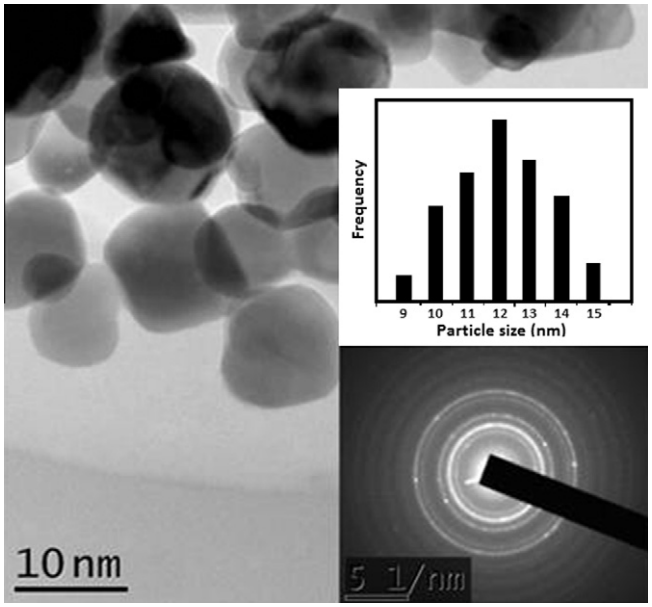

Figure 2. Transmission electron micrograph (TEM) image of 12 nm sized $Ni_xCo_{1-x}Fe_2O_4$ ($x \approx 0.3$) nanoparticles. The inset figures show the selected area electron diffraction (SAED) pattern and histogram of the sample showing the crystalline nature and size-distribution in the samples.

smaller than the particle size obtained from TEM analysis. In our study, we have correlated the magnetization data with the particle size rather than the crystallite size. The average particle size and size distribution was characterized by TEM observations, as shown in Figure 2. The size distribution was obtained by calculating the frequency of a particular selected size in the TEM images; this data was plotted as a particle-size versus frequency histogram (inset of Figure 2). The selected area electron diffraction (SAED) pattern of the samples (shown in the inset of Figure 2) indicates the polycrystalline nature of the nanoparticles. Figure 3 shows the energy dispersive spectroscopy (EDS) results for the nanoparticles; the spectrum indicates the presence of Ni, Co, Fe, and oxygen in the samples. The quantitative results are shown in Table 1, from which it can be observed that Co and Ni are present in 14 and 6 weight percents, thereby indicating their presence as 30% and 70% in accordance with the initial stoichiometric ratios used. Similarly,

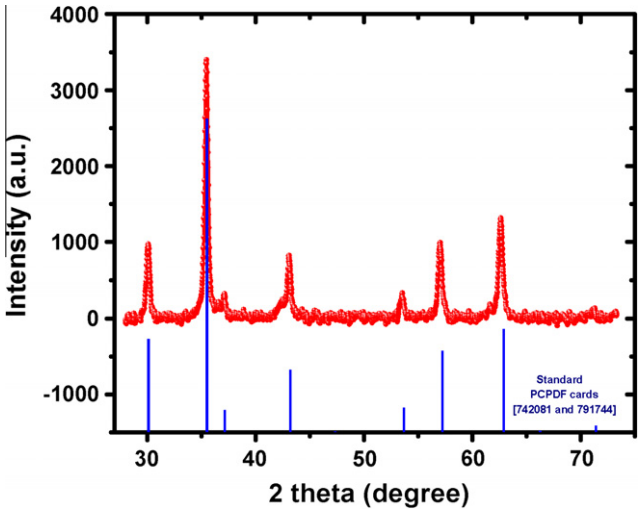

Figure 1. X-ray diffraction (XRD) patterns of $Ni_xCo_{1-x}Fe_2O_4$($x \approx 0.3$) nanoparticles annealed at 600 °C for 6 h with average particle size of ~12 nm.

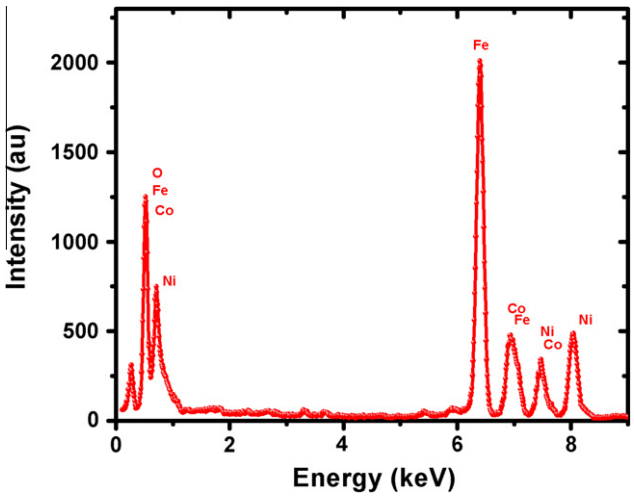

Figure 3. Energy dispersive spectroscopy (EDS) results of nickel–cobalt ferrite nanoparticles.

Table 1
Quantitative results of energy dispersive spectroscopy (EDS) showing weight and atomic percentage of Fe, Co, Ni, and oxygen in the nanoparticles.

Element line	Weight%	Weight% error	Atomic%	Atom% error
O	32.46	±0.39	63.03	±0.76
Fe	47.01	±0.39	26.15	±0.22
Co	14.02	±0.29	7.72	±0.10
Ni	6.51	±0.11	3.10	±0.05
Total	100.0		100.0	

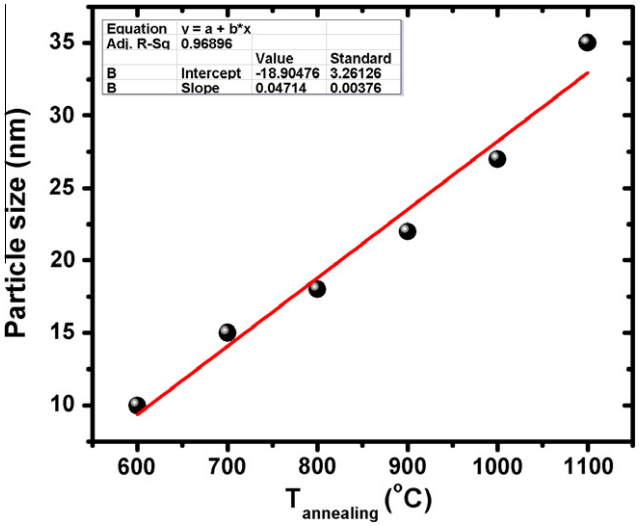

Figure 4. Particle size as function of annealing temperature for $Ni_{0.3}Co_{0.7}Fe_2O_4$ nanoparticles. The red line indicates the linear fit to the experimental data. (For interpretation of the references to color in this figure legend, the reader is referred to the web version of this article.)

the atomic percentages shown in the table indicate proportions of 3:7 for nickel and cobalt in the samples. Figure 4 shows the particle growth as function of annealing temperature; the red line indicates the linear fit to the experimental data points. The average particle size of the samples annealed at 600, 700, 800, 900, 1000, and 1100 °C for 6 h were found to be 12, 15, 18, 22, 27, and 35 ± 3 nm, respectively. The figure shows that the particle size increases almost linearly with the annealing temperature within the given temperature range (600–1100 °C). It has been reported earlier that the annealing process normally reduces the lattice strains and defects; however, it can also cause coalescence of smaller grains, thereby resulting in the increase in the average grain size of the particles [13]. Thus, particle size can be controlled by varying the temperature of the samples during the annealing process.

The magnetic characterization of $Ni_{0.3}Co_{0.7}Fe_2O_4$ nanoparticles was performed by PPMS at room temperature (300 K) and 10 K. Figure 5a–c shows the magnetization hysteresis $M(H)$ loops for the 12-, 18-, and 35-nm samples. The red curves represents the $M(H)$ loops obtained at 10 K with a maximum applied field of up to 20 kOe, and the black curves indicate these loops at 300 K under a 10 kOe field. From the $M(H)$ curves, the coercivity (H_C) at 300 K for sample sizes of 12, 18, and 35 nm were found to be 591, 965, and 438 Oe, whereas at 10 K these values were found to be 5984, 9035, and 5560 Oe, respectively. The saturation magnetization (M_S) at room temperature was found to be 37, 48, and 58 emu/g, and these values are smaller than the bulk value of ~80 emu/g for $CoFe_2O_4$ while at 10 K these values were found to be 41, 55, and 70 emu/g. It can be observed that both the coercivity and saturation magnetization at 10 K increased substantially. Moreover, the coercivity at 10 K increased by an order of magnitude. The very large values of coercivity at 10 K are consistent with the pronounced growth of magnetic anisotropy, thereby inhibiting the alignment of the moment along the applied field direction. The increasing coercivity with decreasing temperature can be understood by considering the effect of thermal fluctuation of the blocked moment across the anisotropy barriers. The coercivity of the nanoparticles calculated from the $M(H)$ loops was plotted as a function of particle size at 300 and 10 K, as shown in Figure 6. For smaller sizes (12–18 nm), the coercivity at 300 K increased

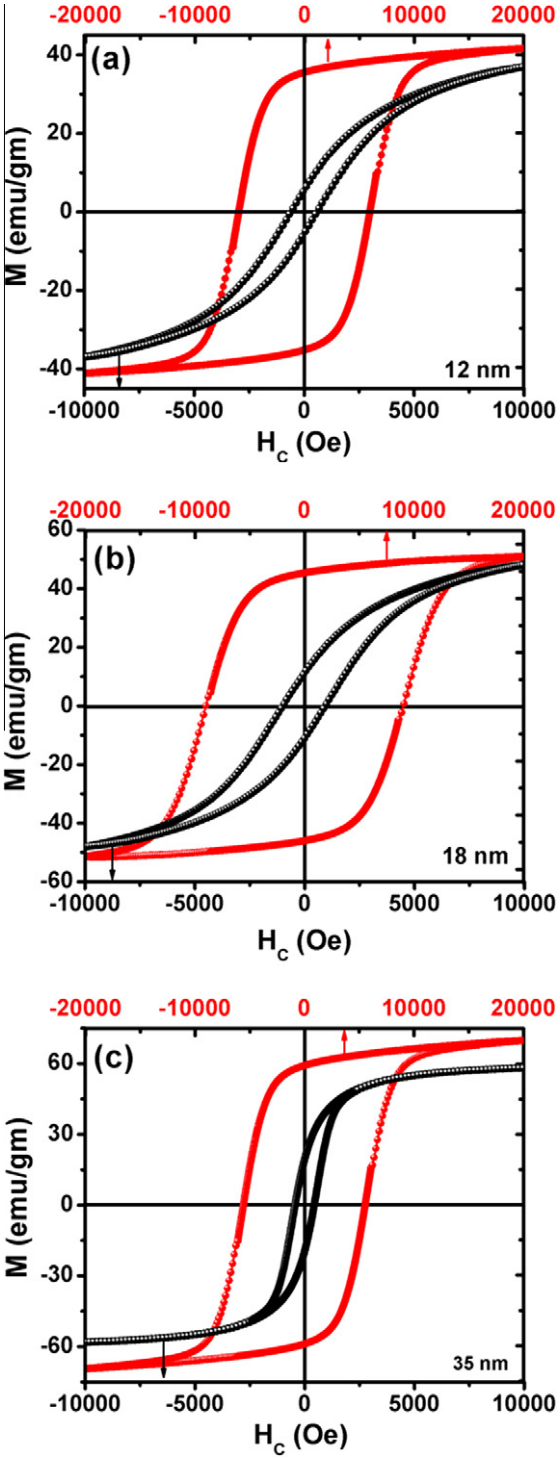

Figure 5. Hysteresis loops for nanoparticles. (a–c) Shows hysteresis loops for 12-, 18-, and 36-nm nanoparticles, respectively, at 300 K (black curve) and 10 K (red curve) at maximum applied field of 10 and 20 kOe, respectively. (For interpretation of the references to color in this figure legend, the reader is referred to the web version of this article.)

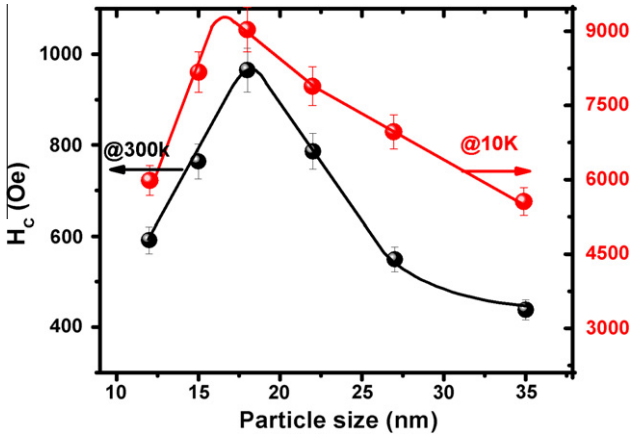

Figure 6. Coercivity (H_C) as function of particle size at 300 K (black line) and 10 K (red line). Both peaks at 300 and 10 K in the curves are evident. (For interpretation of the references to color in this figure legend, the reader is referred to the web version of this article.)

rapidly with size, attaining a maximum value of 965 Oe at a size ($d_{sd} \sim 18$ nm) and then decreased with further increase in particle sizes (18–35 nm). A similar behavior of coercivity was observed at 10 K, with the peak value at about 16 nm. The initial increase in coercivity with d (below the peak) may be assigned to the departure from the superparamagnetic state of the nanoparticles (i.e., transformation from the unblocked to the blocked state). This transformation occurs in smaller nanoparticles when the anisotropy energy dominates the thermal energy in the system. Hence, in the lower d-region (12–18 nm), the coercivity may increase with increasing sizes as the larger particles present in the samples would tend to show a blocked moment. The decline in H_C with increasing d, above d_{sd}, can occur due to two different mechanisms. Firstly, the particle size can become sufficiently large to sustain the domain wall. In this situation, magnetization reversal would occur via domain wall motion, and consequently, a lowered coercivity would be observed. Secondly, the decline in coercivity may be due to the varying role of the surface and its associated anisotropies with diminishing particle size above the peak. Bodker et al. [14] have shown that the effective anisotropy constant increases with decreasing particle sizes according to the expression for spherical nanoparticles as

$$K_{eff} = K_V + (6/d)K_S \quad (1)$$

Here, K_{eff}, K_V and K_S denote the effective, volume, and surface anisotropy constants, respectively. In Figure 6, with decreasing d values from 35 nm, the role of the surface and its associated anisotropy energy is increased. This would tend to increase the coercivity within the Stoner–Wohlfarth law ($H_C = 2K/M_S$), which is consistent with the observed behavior of H_C with respect to d, provided that all the nanoparticles are in the single-domain state, necessary for this law. However, this increase in H_C will not continue indefinitely; as the particle size decreases to a sufficiently small value ($d_{sd} \sim 18$ nm), thermal effects are expected to take over. For the particles below d_{sd}, the thermal energy becomes sufficient to overcome the volume dependent anisotropy energy ($K_{eff}V$), enabling the easier reversal of the moments, thereby leading to the lower critical fields for these small-size nanoparticles [15,16]. This leads to decreasing coercivity in the smaller regime (12–18 nm). The former effect (increased coercivity) is expected in $CoFe_2O_4$ nanoparticles for the sizes close to 50 nm (significantly higher than the critical size of ~18 nm in our case). Therefore, this effect is considered more likely valid for the explanation of the H_c–d curve in our case. The error bars in Figure 6 indicate a clear difference within the experimental data points.

Furthermore, it is observed in Figure 6 that the critical single-domain size at 10 K is smaller than that at 300 K. In order to understand this (decreasing) behavior of d_{sd} at 10 K, we consider the following relation [17]:

$$d_{sd} = d(T/T_b)^{1/3} \quad (2)$$

According to Eq. (2), as T decreases, the critical single domain size (d_{sd}) of the nanoparticles decreases. Hence, the peak in H_c–d curve shifts from larger to smaller sizes as the temperature is decreased from 300 to 10 K. The decrease in d_{sd} at 10 K can also be ascribed to the exchange-coupling effects that play a prominent role at lower temperatures in core–shell nanoparticles [18]. In our case, the exchange coupling is expected to be observed directly in the core and shell of the nanoparticles as they comprise ferrimagnetic cores surrounded by the antiferromagnetic Ni- and/or Co-oxide shells. The core–shell nature of our nanoparticles can also cause another important effect known as the *exchange bias* effect, which is of great scientific and technological interests and can be studied in these nanoparticles.

Figure 7 shows the saturation magnetization as a function of particle size at 300 K. The saturation magnetization for 12–35 nm sizes varies between 37 and 58 emu/g. The graph shows that the saturation magnetization increases as the size of the particles increases. The observed increase in M_S with increasing values of d may be attributed to the increase in the core size of the nanoparticles responsible for magnetization in the samples. For smaller nanoparticles, because of the smaller size of the cores, the saturation magnetization is smaller while it is larger for larger particles due to the correspondingly larger core size. For larger nanoparticles (above 18 nm) the role of the surface is going to decrease. Therefore, the main contribution towards the increasing saturation magnetization in this case would be arising from the core–shell effects. However, the contribution due to the surface anisotropy cannot be excluded as well.

We studied the superparamagnetic blocking behavior as a function of particles size for these nanoparticles. Figure 8 shows the blocking temperature T_b as a function of d as derived from the $M(T)$ curves of the samples. The inset of the figure shows a typical zero-field cooled (ZFC) $M(T)$ curve for one of the representative samples (18 nm). For a single particle at finite T, the ferromagnetically aligned magnetic moments fluctuate between their two energetically degenerate ground states on a time scale given by the following relation [19]:

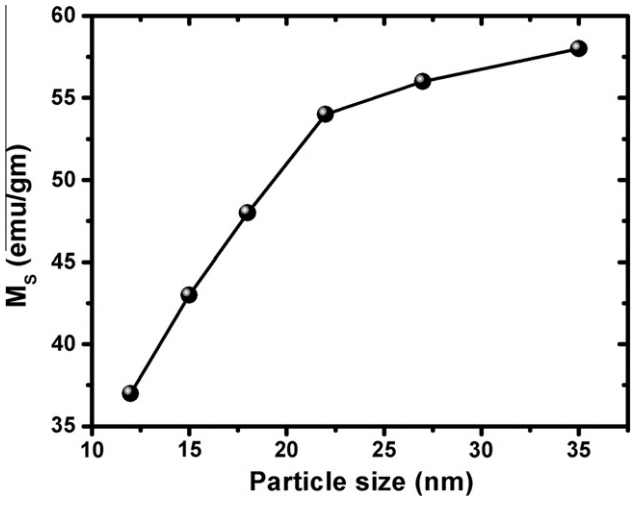

Figure 7. Saturation magnetization (M_S) as function of particle size for $Ni_{0.3}Co_{0.7}Fe_2O_4$ nanoparticles. The observed values lie considerably below the bulk M_S value of cobalt ferrite.

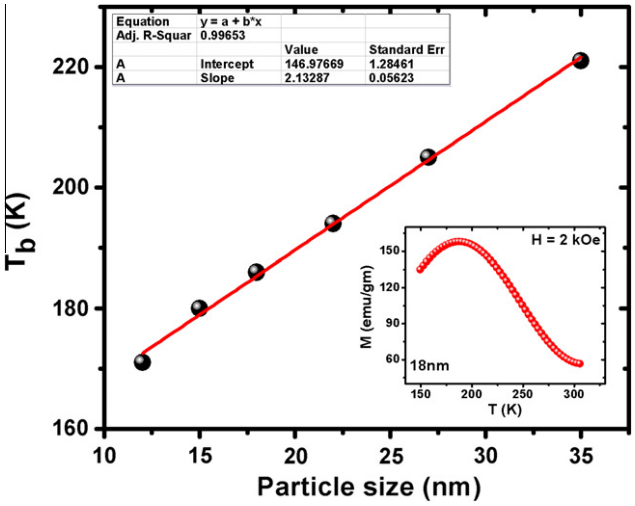

Figure 8. Dependence of blocking temperature T_b on particle size for $Ni_xCo_{1-x}Fe_2O_4$ ($x \approx 0.3$) nanoparticles. The inset shows the zero-field cooled (ZFC) $M(T)$ curves of the samples under applied field of 2 kOe.

$$\tau = \tau_o \exp(K_{eff}V/k_BT) \quad (3)$$

Here, τ denotes the relaxation time and $K_{eff}V$ denotes the effective anisotropy energy of the particles. The term T_b denotes the temperature at which $\tau = \tau_m$, the measurement time of the instrument (VSM). For a finite temperature $T > T_b$, the particle behaves like a superparamagnet (unblocked state). On the other hand, when $T < T_b$, the particle is in the blocked state, i.e., it behaves like a ferromagnet. Referring back to our data (Figure 8), we observe a linear dependence of T_b on d. The larger particles are blocked at high temperatures as compared to the smaller particles. For larger particles, the larger volume causes high anisotropy energy ($K_{eff}V$) of the system, which decreases the probability of a jump across the anisotropy barrier. Hence, the blocking is shifted towards the higher temperatures for larger particles. It is observed in the inset of Figure 8 that the ZFC peak is broad, and this broadness can be either due to the size distribution in the samples or due to the presence of exchange and/or interparticle dipole–dipole interactions among the nanoparticles. These possibilities can be true for our samples; however, the broadness of the peak can be ascribed mainly to the contribution of the exchange and dipolar interactions as the nanoparticles are sintered together forming bigger nanoparticles. A close examination of Figure 2 also confirms that there are aggregated particles present in the samples. Thus, in this case, T_b corresponds to the overall blocking behavior of the nanoparticles assembled together rather than the superparamagnetic blocking temperature of the isolated (non-interacting) nanoparticles [20,21]. However, the actual superparamagnetic blocking temperature is expected to be proportional to T_b in our samples. It is seen that T_b varies almost linearly with particle size as shown in Figure 8 which is different from the behavior expected from Eq. (3). Such deviation from the theoretical results has also been previously reported in $MgFe_2O_4$ and $Li_{0.5}Fe_{2.5}O_4$ nanoparticles [22,23].

4. Conclusion

In this Letter, we have presented a method for synthesis of crystalline $Ni_{0.3}Co_{0.7}Fe_2O_4$ nanoparticles using chemical co-precipitation. The particle size was found to increase linearly with annealing temperature due to the coalescence of smaller grains that resulted in larger grains during annealing. The room temperature coercivity of the samples showed a peak at a critical size $d_{sd} \sim 18$ nm. The behavior of the H_C vs. d above d_{sd} has been attributed to either the domain transformation mechanism in this regime or due to the enhancing role of the surface and its associated anisotropies, whereas below d_{sd}, the variation in H_C has been ascribed to the superparamagnetic blocking effects in the samples. The saturation magnetization tended to increase with particle size (d), which was attributed to the increasing core sizes of the nanoparticles. A high blocking temperature was observed for larger particles due to the high volume-dependent anisotropy energy that causes the particles to be blocked at higher temperatures.

Acknowledgment

This research was supported by the World Class University program funded by the Ministry of Education, Science and Technology through the National Research Foundation of Korea (R32-10204).

References

[1] P. Tartaj, M.D. Morales, V.V. Sabino, J. Phys. D 36 (2003) R-182.
[2] S.D. Bader, Rev. Mod. Phys. 78 (2006) 1.
[3] C.A. Ross, Ann. Rev. Mater. Res. 31 (2001) 203.
[4] C.J. Brumlik, C.R. Martin, Anal. Chem. 59 (1992) 2625.
[5] Z. Cai, C.R. Martin, J. Am. Chem. Soc. 111 (1989) 4138.
[6] S.K. Chakravarti, J. Vetter, Nucl. Instrum. Meth. B 62 (1991) 109.
[7] M. Naeem, S. Qaseem, I. Ahmad, M. Maqbool, J. Nanopart. Res. 14 (808) (2012) 01.
[8] I.M.L. Billas, A. Chatelain, W.A. de Heer, Science 265 (1994) 1682.
[9] D.D. Awschalom, D.P.D. Vincenzo, Phys. Today 43 (1995).
[10] S. Son, M. Taheri, E. Carpenter, V.G. Harris, M.E. McHenry, J. Appl. Phys. 91 (10) (2002) 7589.
[11] V. Pallai, D.O. Shah, J. Magn. Magn. Mater. 163 (1996) 243.
[12] T. Feried, G. Shemer, G. Markovich, Adv. Mater. 13 (15) (2001) 1158.
[13] T.P. Raming, A.J.A. Winnubst, C.M. van Kats, P. Philipse, J. Colloid Interface Sci. 249 (2002) 346.
[14] F. Bodker, S. Morup, S. Linderoth, Phy. Rev. Lett. 72 (1994) 282.
[15] H. Pfeiffer, Phys. Stat. Sol. (a) 118 (1990) 295.
[16] R. Christy, Z.J. Vestal, Nano Lett. 3 (1) (2003) 1739.
[17] B.D. Cullity, Introduction to Magnetic Materials, Addison-Wesley Publishing Company Inc, Reading, MA, 1972.
[18] M. Vazquez, C. Luna, M.P. Morales, R. Sanz, C.J. Serna, C. Mijangos, Physica B 354 (2004) 71.
[19] A. Aharoni, Introduction to the Theory of Ferromagnetism, Clarendon Press, Oxford, 1996. p. 94.
[20] Y. Zhang et al., J. Appl. Phys. 108 (2010) 084312.
[21] G.C. Papaefthymiou, E. Devlin, A. Simopoulos, Phys. Rev. B 80 (2009) 024406.
[22] Sagar.E. Shirsath, R.H. Kadam, A.S. Gaikwad, Ali Ghasemi, Akimitsu Morisako, J. Magn. Magn. Mater. 323 (23) (2011) 3104.
[23] Qi. Chen, Appl. Phys. Lett. 73 (1998) 3156.